Tuning the electronic properties of armchair carbon nanoribbons by a selective boron doping

2010 J. Phys.: Condens. Matter 22 505302

(http://iopscience.iop.org/0953-8984/22/50/505302)

IOP Publishing Journal of Physics: Condensed Matter

J. Phys.: Condens. Matter **22** (2010) 505302 (9pp) doi:10.1088/0953-8984/22/50/505302

Tuning the electronic properties of armchair carbon nanoribbons by a selective boron doping

P Navarro-Santos[1], J L Ricardo-Chávez[1], M Reyes-Reyes[2], J L Rivera[3,4] and R López-Sandoval[1]

[1] Instituto Potosino de Investigación Científica y Tecnológica, Camino a la presa San José 2055, San Luis Potosí 78216, Mexico
[2] Instituto de Investigación en Comunicación Óptica, Universidad Autónoma de San Luis Potosí, Alvaro Obregón 64, San Luis Potosí 78000, Mexico
[3] Facultad de Ingeniería Química, Universidad Michoacana de San Nicolás de Hidalgo, Santiago Tapia 403, Morelia, Michoacán, 58000, Mexico
[4] Instituto de Investigaciones en Materiales, Universidad Nacional Autónoma de México, Circuito exterior s/n, CU, Del. Coyoacán, 04510, México D.F., Mexico

E-mail: sandov@ipicyt.edu.mx

Received 13 August 2010, in final form 15 October 2010
Published 24 November 2010
Online at stacks.iop.org/JPhysCM/22/505302

Abstract

Armchair carbon nanoribbons (ACNRs) substitutionally doped with boron atoms are investigated in the framework of first-principles density functional theory. Different boron–boron arrangements and concentrations are considered in order to simulate possible aggregation patterns, their structural stability and electronic behavior are determined as a function of ribbon size. In agreement with previous studies, our results show that the dopant atoms have in general a preference for edge sites, but specific effects appear as a function of concentration that importantly modify the properties of the ribbons compared to the pristine case. Interesting tendencies are discovered as a function of dopant concentration that significantly affect the electronic properties of the ribbons. We have found that BC_3 island formation and edge doping are the most important factors for the structural stabilization of the ribbons with high boron concentration ($>7\%$) whereas for the cases of low boron concentrations ($<5\%$) the structural stabilities are similar. For all the doped cases, we have found that the BC_3 island patterns give rise to highly localized B states on top of the Fermi level, resulting in semiconducting behavior. On the other hand, when the average distance between the B atoms increases beyond island stoichiometry, the localization of their states is reduced and the ribbons may become metallic due to a band crossing caused by the lowering of the Fermi level resulting from the positive charge doping. Thus, tuning the dopant interaction would be an appropriate way to tailor the electronic properties of the ribbons in a convenient manner in view of potential technological applications.

(Some figures in this article are in colour only in the electronic version)

1. Introduction

Recent advances in experimental and theoretical techniques to study the properties of nanometric materials have shown a subtle dependence on their geometry and composition, in such a way that it is possible now to devise new ways to build materials simply by modifying these parameters. In particular, carbon shows an extraordinary capacity to adopt different geometrical structures, leading to a large variety of materials with novel physical properties. Some of these structures, like carbon nanotubes, graphene and carbon nanoribbons, have

attracted a lot of interest due to the feasibility of tailoring their structural and electronic properties [1–6].

Carbon nanoribbons (CNRs) are quasi-one-dimensional infinite carbon sheets with sp^2 bonding. Depending on the cut orientation, it is possible to obtain two different topological conformations, usually called armchair (ACNRs) and zigzag (ZCNRs), where edges play an important role on the electronic properties [4–13]. Experimentally, CNRs can be synthesized by chemical techniques or by mechanical, electrical and chemical exfoliation of graphite and carbon nanotubes [14–24]. Although these techniques may produce ribbons with high degree of edge disorder, in most theoretical works the ribbon edges are supposed to be of ideal shape passivating them with hydrogen to eliminate the dangling bonds and increase the stability [25]. Theoretical studies have shown that, in contrast to the properties of carbon nanotubes where the topology determines solely the semiconducting or metallic behavior, all hydrogen-passivated CNRs are semiconducting independently of the nature of the edges [11]. Nevertheless, it has been shown that a selective doping, either with acceptor or donor impurities, may change the electronic properties in a suitable way for technological applications [14, 26–28]. The structural, magnetic, and electronic properties of doped CNRs have been widely studied in recent years as a function of width and chirality [4–6, 10, 11, 29–31]. Most of these studies have focused principally on zigzag topology since it has been shown that ZCNRs are especially interesting due to a large contribution to the local density of states near the Fermi level (E_F) coming from localized edge states, and these states are responsible for the magnetization at the edges [6, 11, 30, 31]. However, to our knowledge, there are no systematic studies of the effects of the interaction between several impurities on the structural and electronic properties of CNRs. In particular, we have focused on ACNRs because their electronic structures are simpler than those of ZCNRs and the effects of different boron patterns are easier to grasp. Moreover, it is well established that substitutionally doping carbon nanotubes with B impurities leads to a remarkable preference for zigzag chirality [15] and that zigzag carbon nanotubes unfold into ACNRs. Therefore, a possible route to synthesize B-doped ACNRs could be by using the following procedure: (i) producing boron-doped carbon nanotubes in an arc-discharge dc generator [15–17] or by substitution reactions of carbon atoms in pristine carbon nanotubes [18]; (ii) cutting these B-doped structures into nanoribbons using a chemical oxidation, argon plasma etching or electrical current [22–24].

We have investigated the way the interaction between several dopant atoms, resulting from their relative spatial arrangement, modifies the structural and electronic properties of boron-doped ACNRs. Studies on B-doped carbon nanotubes suggest that the B atoms tend to aggregate forming islands with BC_3 stoichiometry. However, in planar structures these conformations may lead to high local stress and impurity–impurity repulsion compared to a randomly distributed arrangement. To gain insight on how these variables determine the structural stability and electronic behavior, we consider ribbons of different sizes having a constant number of impurities and perform first-principles calculations in the framework of density functional theory (DFT). The structural relaxation of the ribbons is carried out by taking into account different aggregation patterns where the impurity–impurity separation goes from one to several times the nearest-neighbor distance. The main details on the computational methods employed in our calculations are given in section 2, while the actual results are presented in section 3. Finally, in section 4 we summarize the main conclusions of the study.

2. Computational method

The electronic calculations have been carried out using the Vienna *Ab initio* Simulation Package (VASP) [32], which provides an efficient implementation of the Kohn–Sham scheme of DFT in an augmented plane-wave basis set. The interactions between valence electrons and ionic cores are taken into account by means of the projector augmented wave (PAW) method [33], while the electronic exchange and correlation effects can be treated in a variety of ways. In particular, we have used the generalized gradient approximation (GGA) in the form proposed by Perdew–Burke–Ernzerhof (PBE) [34]. Since VASP uses a periodic approach to electronic structure by repeating system images on real space, the ribbons are placed in a supercell with lattice vectors $\vec{a}$, $\vec{b}$, and $\vec{c}$ whose magnitudes are chosen so that the interactions between neighboring images along the non-periodic directions $\vec{a}$ and $\vec{c}$ are negligible (see figure1). In practice, this happens when there is at least 10 Å of vacuum separation between the images.

The electronic and structural relaxation of the ribbons was performed self-consistently without imposing any *a priori* restriction by using the conjugated gradient algorithm to find the minimum of the total energy and interatomic forces within a convergence threshold of 1×10^{-4} eV for the energy and 1×10^{-2} eV Å^{-1} for the forces. We searched for spin-polarized and non-spin-polarized solutions of the Kohn–Sham equations but were unable to find significant differences between them [11]. This implies that the non-magnetic state is always the most stable. Therefore, the results reported in section 3 correspond to the non-spin-polarized or paramagnetic case.

3. Results and discussion

We start by considering in the first place a pristine ACNR passivated with hydrogen on the edge atoms. Following the usual convention [13], the size of the ribbons is denoted as $M \times N$, where the width M is the number of dimer chains along the transverse direction, and the length N represents the number of rows along the periodic direction (see figure1). We have studied two different sizes of supercells of widths $M = 16$ (20.4 Å) and $M = 20$ (25.5 Å) respectively, which are characteristic of ribbons having small and large gaps at the Fermi level [11]. We have considered different dopant concentrations by studying ACNRs of lengths $N = 2$ and 4. A schematic representation of the ribbon of 16×2 is shown in figure 1.

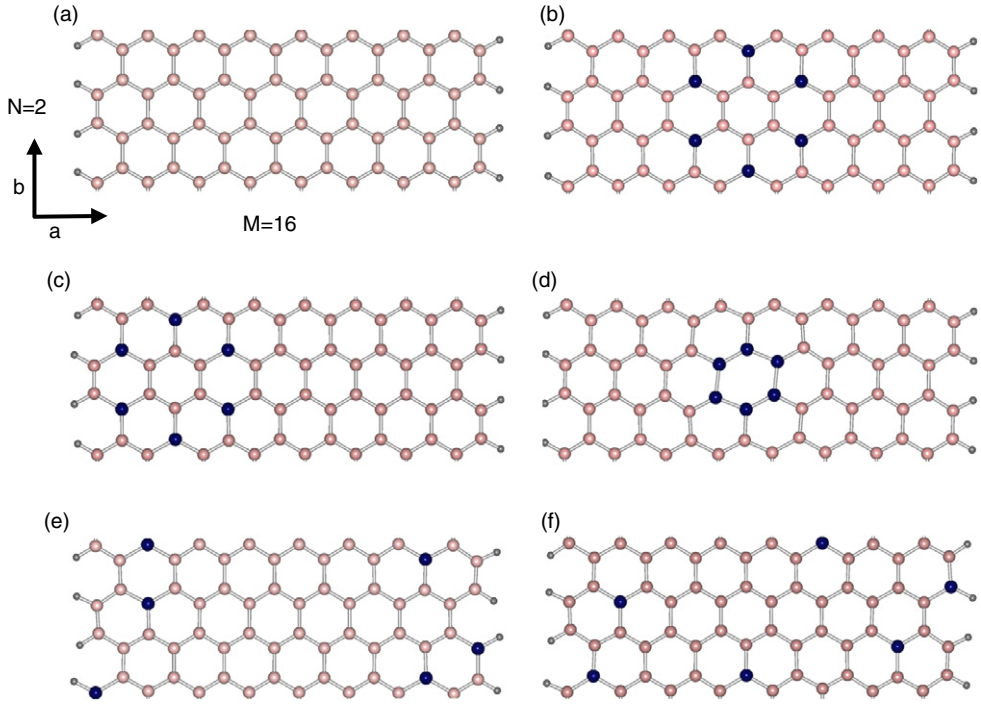

Figure 1. Optimized unit cell geometries of ACNRs of size $M \times N = 16 \times 2$: (a) pristine, (b) ACNR-C, (c) ACNR-E, (d) ACNR-Ri, (e) ACNR-H and (f) ACNR-Ra. Blue (dark) and pink (light) balls represent boron and carbon atoms respectively.

The doped ACNRs were obtained by spatially distributing six substitutional boron atoms over the entire unit cell atomic positions of the pristine ribbon in order to simulate different aggregation patterns. This corresponds to an impurity fraction of around 9.4% ($M = 16$) and 7.5% ($M = 20$) for length $N = 2$, and 4.7% ($M = 16$) and 3.75% ($M = 20$) for $N = 4$ respectively. The considered geometrical arrangements of the ribbon of 16×2 are shown in parts (b)–(f) of figure 1. Parts (b) and (c) are examples of nano-island arrangements of BC_3 stoichiometry as proposed by Carroll *et al* in their study of boron-doped multiwalled carbon nanotubes [16]. In case (b) the island is located at the center of the ribbon and this configuration is denoted as ACNR-C, while in (c) the island is near the edge of the ribbon and this arrangement is denoted as ACNR-E. A special type of nano-island formation, where the boron atoms form a complete substituted ring denoted as ACNR-Ri, is shown in case (d) of figure 1. Taking into account the fact that charge donors or acceptors have a preference for the sites near the edges of the nanoribbon [30], we have added two doping configurations in which the boron atoms are located mainly on the edges (as in case (e) of figure 1, denoted as ACNR-H) and randomly distributed along the entire unit cell (as in case (f) of figure 1, denoted as ACNR-Ra). These arrangements cover the main pathways that could better stabilize the doped ACNRs, these being the tendency to form nano-islands [16], the preference for the ribbon edges where charge transfers could be important [30], and the possibility of adopting conformations reducing the interactions between the dopants [6].

The structure of both pristine and doped ACNRs was optimized by relaxing self-consistently the interatomic distances and cell size. The unit cells of the most stable configurations have parameter values of $a = 26$ Å (width) and $b = 8.72$ Å (length) for $M = 16$, and $a = 30$ Å and $b = 8.72$ Å for $M = 20$ for the case of $N = 2$, while in the case $N = 4$, the optimized unit cell length decreases by up to 0.2 Å with respect to the double size value ($b = 17.44$ Å) due to a lower B concentration. In all cases the final geometries show C–C distances between 1.41 and 1.44 Å, while configurations having BC_3 stoichiometry (cases (b), (c) and (e) of figure 1) show B–C distances of the order of 1.50 Å. The B–B distances vary on average from 1.58 Å for the completely substitutional boron ring (case (d) of figure 1) to 2.97 Å for the cases with BC_3 stoichiometry islands, and 4.98 Å the smallest B–B distance for the ACNR-Ra cases. In addition, the distances between BC_3 islands in ribbons with lengths $N = 4$ are larger than those with $N = 2$.

Table 1 shows the cohesive energy per atom and the Gibbs free energy of the pristine and doped ACNRs of width $M = 16$ and 20 of different lengths $N = 2$ and 4. The cohesive energy (E_C) is the energy required to disassemble a system into its constituent parts. A bound (stable) system has a positive value of E_C, which represents the energy gained during the formation of the bound state. These values were obtained by using a Monkhorst–Pack grid of size $1 \times 20 \times 1$ k-points to sample the Brillouin zone. We observe similar tendencies of the E_C of studied ribbons for different M values and the same N value. For all the cases, the least stable conformation is ACNR-Ri, which, as reported by Martins *et al* [6], has the highest repulsion between the boron atoms and for this reason is not reported in the table. For the cases of $N = 2$, we find that the scattered BC_3 cases (ACNR-Ra and ACNR-H) are less stable than the BC_3 island conformations ACNR-C and ACNR-E, which are the most stable conformations.

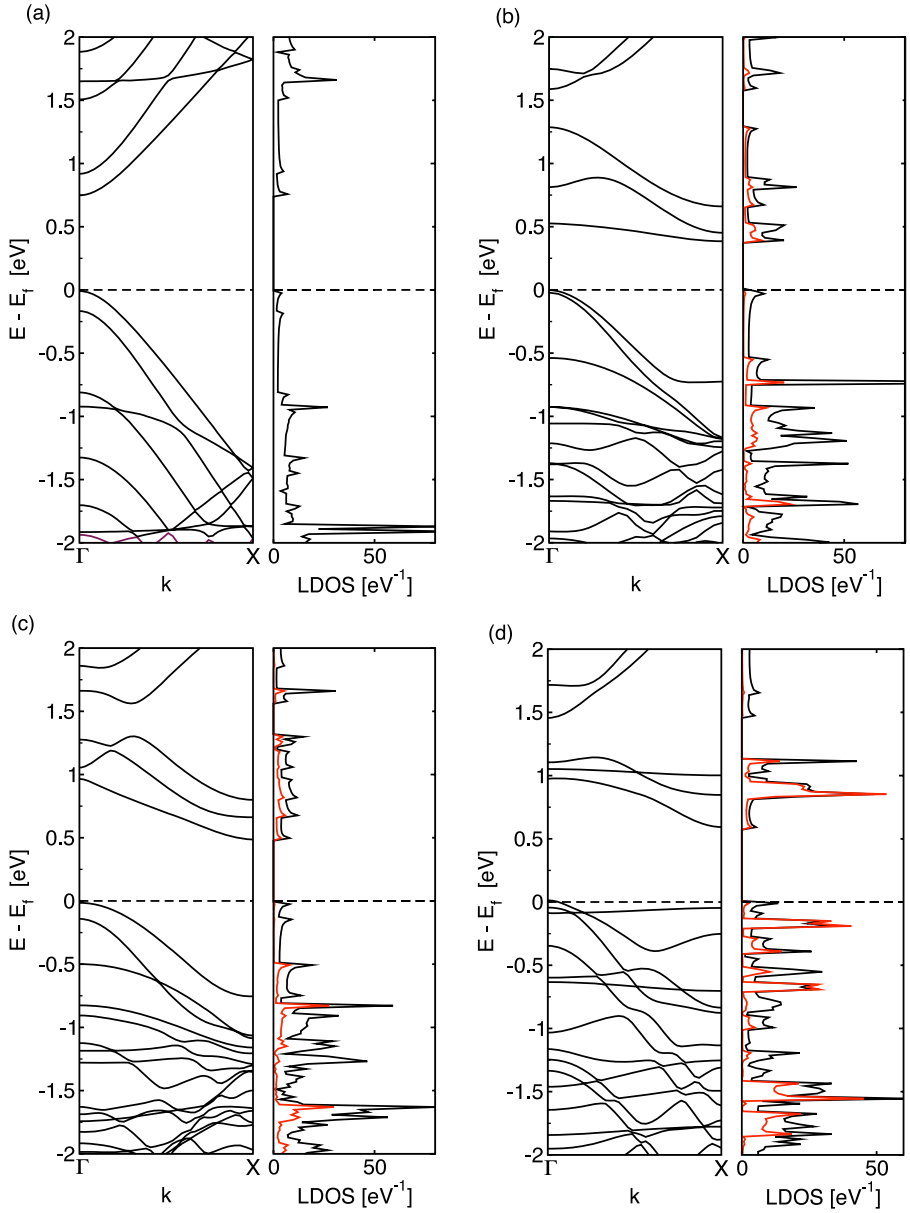

Figure 2. Band structure, total density of states (black line) and local density of states of the boron atoms (red/gray line) of the semiconducting ACNRs of size $M \times N = 16 \times 2$. Part (a) corresponds to the pristine ACNR, while parts (b)–(d) refer to the ACNR-C, ACNR-E, and ACNR-Ri ribbons (see figure 1).

Table 1. Cohesive per atom (Gibbs free) energy in eV of the pristine and B-doped ACNRs whose boron patterns are shown in figure 1.

$M \times N$	Pristine	ACNR-C	ACNR-E	ACNR-H	ANCR-Ra
16×2	7.224 (0.003)	7.003 (−0.291)	7.008 (−0.297)	6.992 (−0.280)	6.983 (−0.272)
20×2	7.338 (0.002)	7.158 (−0.239)	7.161 (−0.242)	7.149 (−0.230)	7.143 (−0.224)
16×4	7.225 (0.003)	7.116 (−0.147)	7.115 (−0.146)	7.118 (−0.149)	7.112 (−0.142)
20×4	7.339 (0.002)	7.250 (−0.120)	7.249 (−0.119)	7.251 (−0.121)	7.249 (−0.119)

In particular, the energy decreases slightly when the island is near the edge of the ribbon, indicating that BC_3 island formation [16] and substitution on the edges [6, 30] are the most important routes to stability. However, in systems where $N = 4$ (<5%) the most stable configuration is found in the ribbon with dopants substituted on the edge forming half islands (ACNR-H). This implies that the distance between the images of the BC_3 islands is another key factor for the stability of these structures. Moreover from table 1, we observe that in low B doping (<5%) the aggregation patterns of the B-doped ACNRs proposed in this work could be possible to synthesize because their cohesive energies are slightly different. Due to the chemical composition of these structures, the E_C could not provide an adequate measure to compare

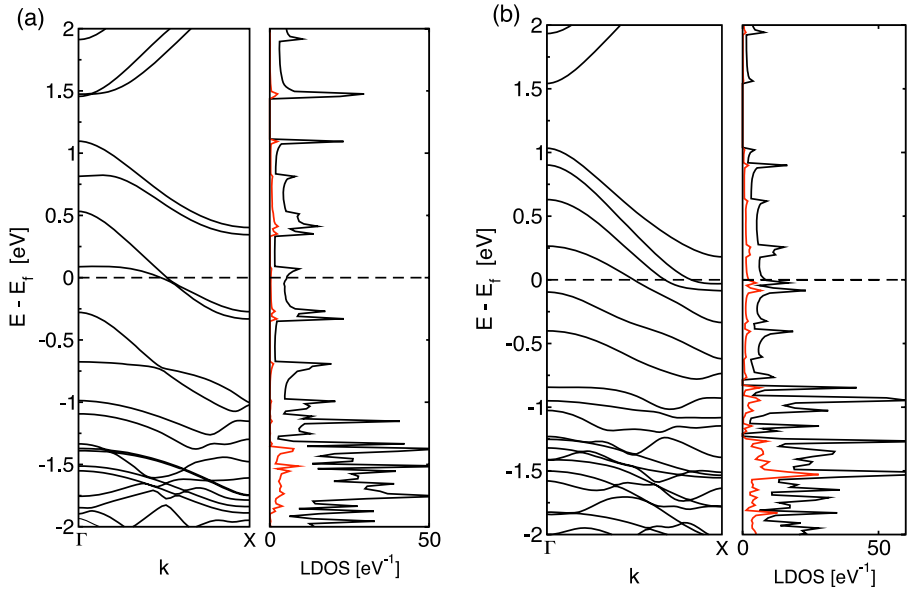

Figure 3. Band structure, total density of states (black line) and local density of states of the boron atoms (red/gray line) of the metallic ACNRs of size $M \times N = 16 \times 2$. Part (a) refers to the ACNR-H ribbon while part (b) corresponds to the ACNR-Ra ribbon (see figure 1).

the relative stability of multicomponent systems like these ACNRs [25, 35]. Therefore, table 1 also shows the Gibbs free energy of formation (δG) of B-doped and pristine ACNRs. This approach has been used in binary phase thermodynamics for taking into account the chemical composition [36]. The molar Gibbs free energy is given by

$$\delta G = E(x) + x_{\mathrm{H}}\mu_{\mathrm{H}} + x_{\mathrm{B}}\mu_{\mathrm{B}} + x_{\mathrm{C}}\mu_{\mathrm{C}} \qquad (1)$$

where $-E(x)$ is the cohesive energy per atom of the ACNR, μ_{H} is the binding energy per atom of the singlet ground state of the H_2 molecule, μ_{B} is the binding energy per atom of the triplet ground state of the B_2 molecule, and μ_{C} is the cohesive energy per atom of the graphene sheet, x_i corresponds to the molar fraction of the different components (H, B, C) which satisfies $\sum x_i = 1$. A negative value of δG represents a stable structure with respect to the constituent whereas a positive value represents a metastable structure. From table 1, we observe that the pristine ACNRs are metastable structures with δG lower than 0.004 eV. These results are in good agreement with other stabilities of pristine nanoribbons reported in the literature [25]. On the other hand, B doping leads to stabilizing energetically the ACNRs of all the configurations proposed in this work.

The electronic properties of the ribbons are inferred from the band structure and the total and local density of states (DOS and LDOS). These quantities were computed by integration over the Brillouin zone using a Monkhorst–Pack grid that is two times denser than in the case of total energy. Additionally, a Gaussian smearing of the energy levels of width 0.02 eV was used to improve the convergence of the integrals. In figures 2 and 3 are exhibited the band structure, DOS and LDOS for both the pristine and doped configurations of the ribbons of size 16×2. Our calculations lead to similar results on the electronic behavior of the other concentrations of doped ACNRs, which shows that the electronic properties depend more on the arrangement between dopants than on the lengths and widths of the cells. Thus we are presenting in this part of our work only the electronic properties of the doped ACNRs 16×2 as an illustrative case.

From part (a) of figure 2 we observe that the pristine ACNR is semiconducting, with an energy gap value at the Fermi level that depends on width M [4, 7, 10, 11]. For $M = 16$ the gap size is $\Delta \sim 0.748$ eV, while for $M = 20$ it is reduced to $\Delta \sim 0.165$ eV. This is in close agreement with results published by Son *et al* [11], who found that hydrogen-passivated ACNRs have a gap size scaling as $\Delta \sim \frac{1}{W}$ as a function of width W, and following a hierarchy $\Delta_{3p+1} > \Delta_{3p} > \Delta_{3p+2}$, where p is a positive integer related to the ribbon width. This hierarchy is associated to the quantum confinement of the electronic states on the transversal section of the ribbon as well as the shortening of the C–C bond lengths near the edges, resulting in an increase of the π–π hopping parameters. Indeed, we find that the C–C bond lengths at the edge atoms are reduced by up to 3.8% compared to the center atoms.

Regarding the effect of B doping on the electronic properties of the pristine ribbons, we observe in general two kinds of trends. On the one hand, there are global modifications of the electronic structure, i.e., present in all doped cases, like a lowering of the Fermi energy E_{F} compared to the pristine ribbon (see cases (b)–(d) of figure 2, and cases (a) and (b) of figure 3). On the other hand, there are specific features related to the relative arrangement of the dopant atoms. For instance, ribbons where the dopant atoms are close together forming islands are semiconducting (like in cases (b), (c), and (d) of figure 2, corresponding to ACNR-C, ACNR-E, and ACNR-Ri ribbons) while ribbons where the dopant atoms are separated away from each other are metallic (see cases (a) and (b) of figure 3, which correspond to ACNR-H and ACNR-Ra ribbons). In the next few paragraphs we discuss these features in more detail.

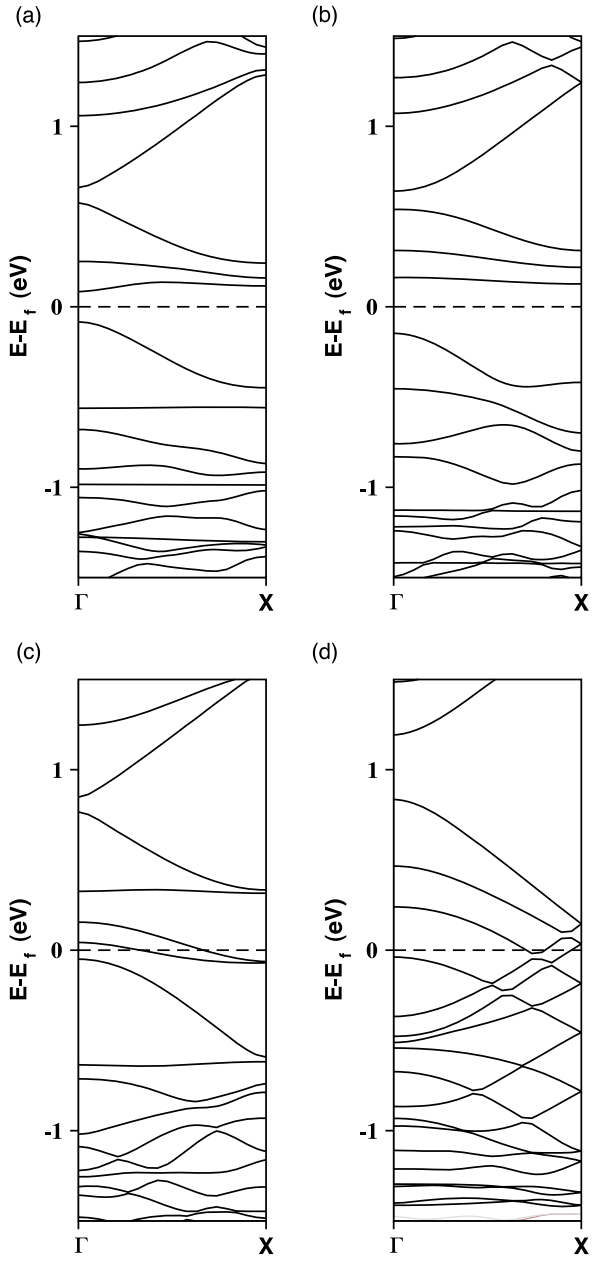

Figure 4. Band structure of the doped ACNRs of size 20 × 4. Part (a) corresponds to the ACNR-C ribbon, while parts (b), (c), and (d) refer to the ACNR-E, ACNR-H, and ACNR-Ra ribbons respectively (see aggregation patterns in figure 1).

First, the lowering of E_F in the doped ACNRs results from the positive charge doping (minus one electron per B atom). Although this is a global feature, the magnitude of the lowering depends non-trivially on the relative arrangement of the dopant atoms and tends to be larger for ribbons where the B atoms form islands due to the opening of an energy gap at E_F. Another gap similar to that of the pristine ribbon is also present in all cases but it is pushed away to the top of the bandwidth by the lowering of E_F and its width is strongly affected by the arrangement of the B atoms. This gap is smaller in the semiconducting ACNRs due to a tendency to form localized B states on top of E_F (look at the contribution of the B atoms to the LDOS and total DOS in cases (b–(d) of figure 2). A limiting case of this behavior is present in the ACNR-Ri ribbon (case (d) of figure 2) where the interaction between the dopant atoms tends to strongly localize the B states close to the Fermi level. These results are in agreement with the work of Charlier *et al* [17], who observed localized peaks near the Fermi level in the DOS of armchair carbon nanotubes having a B-dimer terminated tip. The localization also causes the opening of the energy gap at the Fermi level of the B-doped ACNRs and is responsible of their semiconducting behavior. Thus, ribbons where the dopant atoms aggregate forming islands seem more suitable for field emission devices due to these localized acceptor states close to E_F.

The metallic ACNR-H and ACNR-Ra ribbons share the common characteristic that the boron atoms are separated away from each other and interact very weakly. Although their band structure still shows traces of localized acceptor-state formation near the Fermi level, the B states have also a higher degree of delocalization over the entire energy bandwidth compared to the semiconducting ribbons (parts (a) and (b) of figure 3 and parts (b)–(d) of figure 2). Therefore, the metallic behavior is a consequence of the crossing of some of these delocalized energy bands due to the lowering of the Fermi level resulting from the positive charge doping. Let us stress that this is also a direct consequence of the large distance between the B atoms. Note also that this effect cannot be completely taken into account by a rigid band model, as was suggested in a previous study of B-doped single-wall carbon nanotubes [18]. As we have already mentioned, there are non-negligible modifications to the global electronic structure of the ribbons coming from the dopant atoms. Notice that ACNR-H is an intermediate case between a completely formed BC_3 island and a random B distribution. This case has a slight degree of BC_3 clusterization on the edges and some of their bands on top of E_F tend to localize, at least more than in the ACNR-Ra ribbon where the B atoms are completely delocalized over the entire unit cell.

The electronic structure trends, reported before for high concentration doping (>7%), can be observed in the case of low doping concentration and even in the case where there is only one B impurity. In figure 4 we show the band structure of the B-doped ribbons of size 20 × 4 (3.5% boron concentration). From figure 4, we observe in all cases the lowering of the Fermi energy, whereas in the cases of ACNRs doped with boron nano-islands we found the semiconducting behavior due to localized energy bands above E_F (see parts (a) and (b) of figure 4). In parts (c) and (d) of figure 4, we show the metallic B-doped ribbons and, in the case of part (c) of figure 4, we observe a strong localized acceptor-like band above E_F, which is a consequence of B substitutions on the ribbon edge. However, the metallicity is reached for the crossing of two delocalized bands due to the weak interaction between dopants. This is verified in the random case (part (d) of figure 4), where the energy bands are completely delocalized over the bandwidth, and the metallic behavior is due to the crossing of some energy bands at E_F. Moreover, we present in figure 5 the band structure and density of states of a ribbon of size 12 × 3 doped with a single B impurity, located either at the center or

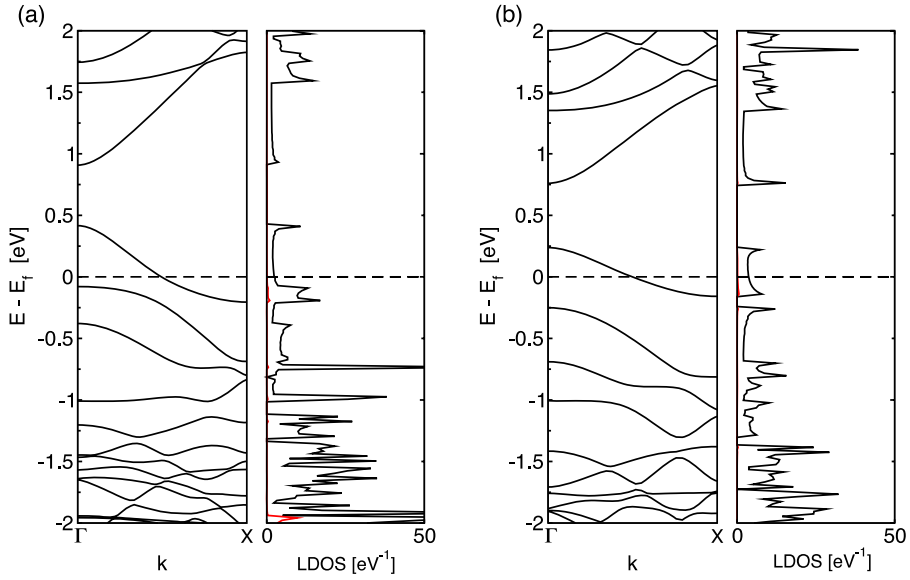

Figure 5. Band structure, total density of states (black line) and local density of states of the boron atoms (red/gray line) of an ACNR of size 12 × 3 with a substitutional B atom located at (a) bulk and (b) edge sites respectively (see [13] for more details).

the edge of the ribbon (parts (a) and (b) of figure 5). These configurations are the same to those analyzed previously by Cervantes-Sodi *et al* [13]. No matter what the lower doping concentration is, the DOS of this ribbon shows the same global features present in the ACNR-H and ACNR-Ra ribbons, i.e., an energy gap on top of E_F which is also present in the DOS of the pristine ribbon and a lowering of E_F that is proportional to the doping charge, giving rise to metallic character due to the crossing of a single energy band at E_F. While the system is metallic in both cases, there is an additional effect when the impurity is at the edge of the ribbon, due to a marked tendency to localize the B states close to the Fermi level, opening a narrow gap below it (see part (b) of figure 5). This result is in contrast to that reported by Cervantes-Sodi *et al*, who observed that the B states tend to strongly localize on top of E_F. The apparent disagreement comes from the fact that in our case the structural relaxation gives average B–C distances of the order of 1.51 Å, while in their case they are of the order of 1.42 Å. As we have already seen, both edge doping and shorter B–C distances are key ingredients for the stabilization of semiconducting ribbons, like in their case. From these results, we deduce that the electronic properties of B-doped carbon nanoribbons with some impurities depend strongly on how the impurities interact with each other. On the one hand, the metallic behavior comes from the weak interaction between dopants, giving rise to delocalized energy bands around E_F. On the other hand, when the average length between dopants is decreased, such as in the cases of boron nano-island arrangements and the extreme case of the completely substituted boron ring, we obtain semiconducting ribbons. In addition, when the B concentration is high it is more probable to obtain ACNRs with boron BC_3 islands and, as a consequence, a semiconductor behavior, whereas if the B concentration is low it is more probable to obtain ACNRs with metallic behavior. From this we conclude that there is a relation among the B patterns, the B concentration and the electronic properties.

Additional information on the influence of the B atoms on the electronic states close to the Fermi level of the ribbons can be obtained by analyzing the spatial distribution of the local density of states at E_F or close to it. This procedure is the theoretical counterpart of an experiment using a scanning tunneling microscope (STM) in the Tersoff–Hamann approximation [37]. In figure 6 we show representative isosurfaces of the partial charge density (PCD) at the Fermi level of the pristine and B-doped ACNRs. Note that in the case of the pristine ribbon (part (a) of figure 6) the PCD is completely delocalized over the entire unit cell atoms, but tends to localize around the B atoms in the doped ribbons, independently of their electronic behavior (see parts (b)–(d) of figure 6). From the local density of states (figures 2 and 3) we deduce that these electrons belong mainly to C atoms, i.e., the B states do not contribute in a significant way to the electronic properties.

4. Conclusions

In this work, we have presented a first-principles study of the electronic properties of high and low B-doped ACNRs in the framework of density functional theory. In contrast to previous studies which mainly considered the effect of a single doping atom, we have included the combined effects of relative position and interaction between several dopants as key variables to develop new ways to build carbon-based materials with novel electronic properties. We have therefore investigated the way the relative arrangement between a given number of B atoms determines the stability and electronic behavior of the ribbons as a function of size. Our results show that, in general, the positive charge doping causes a lowering of the Fermi level of the ribbons compared to the pristine case.

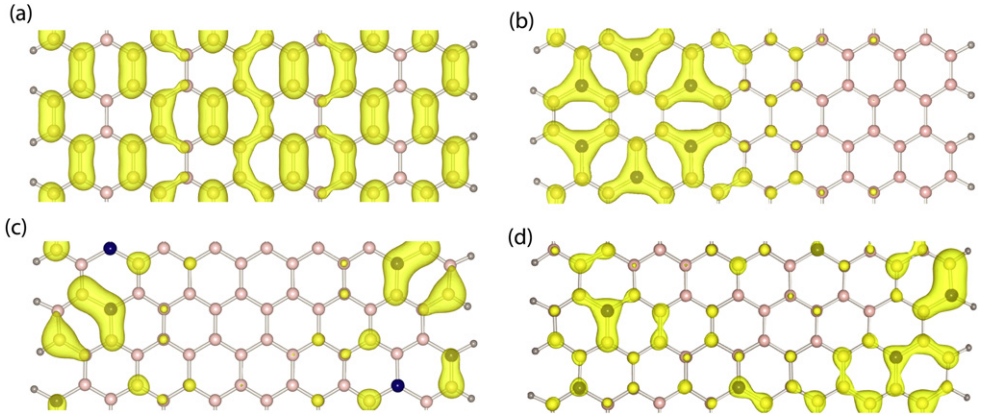

Figure 6. Isosurfaces of the partial charge density at the Fermi level of (a) the pristine ACNR of size $M \times N = 16 \times 2$, and (b)–(d) the corresponding B-doped ACNRs. Part (b) corresponds to the semiconducting ACNR-E ribbon, while parts (c) and (d) refer to the metallic ACNR-H and ACNR-Ra ribbons respectively (see figure 1).

However, this effect cannot be taken into account by a rigid band model, since the B atoms tend to introduce localized acceptor states close to E_F, which may alter in a significant way the electronic behavior.

In particular, we have found that BC_3 island formation and edge doping are the most important factors for the structural stabilization of the ribbons with high B doping concentration (>7%), whereas for low B doping (<5%) ribbons the energetic differences among them are small. Moreover, all doped configurations are thermodynamically stable with respect to their constituents. We have found that a BC_3 stoichiometry strongly modifies the nature of the states close to E_F introducing localized acceptor states and giving rise to semiconducting properties. When the average distance between the dopant atoms is increased the acceptor states are more delocalized over the energy bandwidth but the electronic states near the Fermi level keep a high degree of delocalization. Then, the lowering of E_F gives rise to metallic character since it may cross one or more delocalized energy bands having contributions from both C and B atoms. These results suggest that a selective B doping, varying at the same time the average distance and number of dopants, may be a good way to tailor in a suitable manner the electronic properties of the ACNRs, covering the entire spectrum from semiconducting to metallic behavior. Moreover, these results could point out to experimental researchers what boron distribution they are doping on ACNRs, because the electronic properties of B-doped ACNRs strongly depend on the forming nano-islands and the distance between dopant atoms. Finally, we have analyzed the spatial distribution of the local density of states near E_F to infer how the dopant distribution determines the electronic properties of the ribbons in view of potential technological applications. The results indicate that, independently of the electronic character of the ribbons, the electrons belonging to C atoms close to the dopants are responsible for the electronic properties, i.e, even in the case of metallic ACNRs, these electrons are mostly localized.

Acknowledgments

This work was partially supported by CONACyT (Mexico) under grant numbers S-3148, 48307-R and Fondos Sectoriales-SEP-101263. P Navarro-Santos also thanks CONACyT for financial support under scholarship number 195323. Computer resources were provided by CNS-IPICyT (San Luis Potosí, Mexico).

References

[1] Novoselov K S, Geim A K, Morozov S V, Jiang D, Zhang Y, Dubonos S V, Grigorieva I V and Firsov A A 2004 *Science* **306** 666
[2] Ohta T, Bostwick A, Seyller T, Horn K and Rotenberg E 2006 *Science* **313** 951
[3] Iijima S 1991 *Nature* **354** 54
[4] Nakada K, Fujita M, Dresselhaus G and Dresselhaus M S 1996 *Phys. Rev.* B **54** 17954
[5] Jiang D, Sumpter B G and Dai S 2007 *J. Chem. Phys.* **126** 134701
[6] Martins T B, Miwa R H, da Silva A J R and Fazzio A 2007 *Phys. Rev. Lett.* **98** 196803
[7] Wakabayashi K, Fujita M, Ajiki H and Sigrist M 1999 *Phys. Rev.* B **59** 8271
[8] Lee Y L and Lee Y W 2002 *Phys. Rev.* B **66** 245402
[9] Miyamoto Y, Nakada K and Fujita M 1999 *Phys. Rev.* B **59** 9858
[10] Ezawa M 2006 *Phys. Rev.* B **73** 045432
[11] Son Y W, Cohen M L and Louie S G 2006 *Phys. Rev. Lett.* **97** 216803
[12] Fujita M, Wakabayashi K, Nakada K and Kusakabe K 1996 *J. Phys. Soc. Japan* **65** 1920
[13] Cervantes-Sodi F, Csányi G, Piscanec S and Ferrari A C 2008 *Phys. Rev.* B **77** 165427
[14] Berger C *et al* 2006 *Science* **312** 1191
[15] Blase X, Charlier J-C, De Vita A, Car R, Redlich Ph, Terrones M, Hsu W K, Terrones H, Carroll D L and Ajayan P M 1999 *Phys. Rev. Lett.* **83** 5078
[16] Carroll D L, Redlich Ph, Blase X, Charlier J C, Curran S, Ajayan P M, Roth S and Rühle M 1998 *Phys. Rev. Lett.* **81** 2332
[17] Charlier J C, Terrones M, Baxendale M, Meunier V, Zacharia T, Rupesinghe N L, Hsu W K, Grobert N, Terrones H and Amaratunga G A J 2002 *Nano Lett.* **2** 1191
[18] Fuentes G G, Borowiak-Palen E, Knupfer M, Pichler T, Fink J, Wirtz L and Rubio A 2004 *Phys. Rev.* B **69** 245403
[19] Li X, Wang X, Zhang L, Lee S and Dai H 2008 *Science* **319** 1229

[20] Tapasztó L 2008 *Nat. Nanotechnol.* **3** 397
[21] Datta S S, Strachan D R, Khamis S M and Johnson A T C 2008 *Nano Lett.* **8** 1912
[22] Kosynkin D V, Higginbotham A L, Sinitskii A, Lomeda J R, Dimiev A, Price B K and Tou J M 2009 *Nature* **458** 872
[23] Jiao L, Zhang L, Wang X, Diankov G and Dai H 2009 *Nature* **458** 877
[24] Kim K, Sussman A and Zettl A 2006 *ACS Nano* **4** 1362
[25] Barone V, Hod O and Scuseria G E 2006 *Nano Lett.* **6** 2748
[26] Novoselov K S, Geim A K, Morozov S V, Jiang D, Katsnelson M I, Grigorieva I V, Dubonos S V and Firsov A A 2005 *Nature* **438** 197
[27] Zhang Y, Tan Y, Stormer H L and Kim P 2005 *Nature* **438** 201
[28] Berger C *et al* 2004 *J. Phys. Chem.* B **108** 19912
[29] Dutta S and Pati S K 2007 arXiv:0712.4130v1 [cond mat]
[30] Yu S S, Zheng W T, Wen Q B and Jiang Q 2008 *Carbon* **46** 537
[31] Ding Y, Wang Y and Ni J 2009 *Appl. Phys. Lett.* **94** 073111
[32] Kresse G and Hafner J 1993 *Phys. Rev.* B **47** 558
Kresse G and Furthmüller J 1996 *Phys. Rev.* B **54** 11169
http://cms.mpi.univie.ac.at/vasp
[33] Blochl P E 1994 *Phys. Rev.* B **50** 17953
Kresse G and Joubert D 1999 *Phys. Rev.* B **59** 1758
[34] Perdew J P, Burke K and Ernzerhof M 1996 *Phys. Rev. Lett.* **77** 3865
[35] Hod O, Barone V, Peralta J E and Scuseria G E 2007 *Nano Lett.* **8** 2295
[36] Dumitrica T, Hua M and Yakobson B I 2004 *Phys. Rev.* B **70** 241303
[37] Tersoff J and Hamann D R 1985 *Phys. Rev.* B **31** 805